Imaging the Intact Mouse Cornea Using Coherent Anti-Stokes Raman scattering (CARS)

David A. Ammar,[1] Tim C. Lei,[2] Malik Y. Kahook,[1] and Omid Masihzadeh[1]

[1]Department of Ophthalmology, University of Colorado Denver, Aurora, Colorado
[2]Department of Electrical Engineering, University of Colorado Denver, Denver, Colorado

Correspondence: Omid Masihzadeh, University of Colorado Medical School, Department of Ophthalmology, Mail Stop #8311, 12800 East 19th Avenue, Room #5115, Aurora, CO 80045;
Omid.Masihzadeh@ucdenver.edu.

PURPOSE. The aim of this study was to image the cellular and noncellular structures of the cornea and limbus in an intact mouse eye using the vibrational oscillation of the carbon–hydrogen bond in lipid membranes and autofluorescence as label-free contrast agents.

METHODS. Freshly enucleated mouse eyes were imaged using two nonlinear optical techniques: coherent anti-Stokes Raman scattering (CARS) and two-photon autofluorescence (TPAF). Sequential images were collected through the full thickness of the cornea and limbal regions. Line scans along the transverse/sagittal axes were also performed.

RESULTS. Analysis of multiple CARS/TPAF images revealed that corneal epithelial and endothelial cells could be identified by the lipid-rich plasma membrane CARS signal. The fluorescent signal from the collagen fibers of the corneal stroma was evident in the TPAF channel. The transition from the cornea to sclera at the limbus was marked by a change in collagen pattern (TPAF channel) and thickness of surface cells (CARS channel). Regions within the corneal stroma that lack collagen autofluorescence coincided with CARS signal, indicating the presence of stromal fibroblasts or nerve fibers.

CONCLUSIONS. The CARS technique was successful in imaging cells in the intact mouse eye, both at the surface and within corneal tissue. Multiphoton images were comparable to histologic sections. The methods described here represent a new avenue for molecular specific imaging of the mouse eye. The lack of need for tissue fixation is unique compared with traditional histology imaging techniques.

Keywords: cornea, corneal stroma, coherent anti-Stokes Raman scattering (CARS)

Multiphoton microscopy (MPM) has become a ubiquitous laboratory tool for imaging corneal structures without the use of exogenous fluorophores. Since excitation by MPM only occurs at a small focal volume, it offers intrinsic axial cross-sectioning and image resolution similar to confocal microscopy.[1] Piston et al. showed that corneal two-photon autofluorescence[2] (TPAF) is generated by collagen within the stroma as well as by reduced nicotinamide adenine dinucleotide (NAD[P]H) contained within the individual basal epithelial cells.[3] Subsequent studies were able to use second-harmonic generation[4,5] (SHG) to image individual collagen fibers within the stroma.[6-8] These imaging techniques have been validated through the use of exogenous fluorescence tags,[9] as well by their ability to identify manifestations of corneal inflammation, keratoconus, and stromal edema in various animal models.[10-12] While these multiphoton-imaging techniques can give information on the tissue structure of the cornea, they cannot image the cell membranes in the way possible with single photon laser scanning confocal microscopes.[13]

All MPM involves simultaneous interactions of multiple photons with a target molecule to generate a signal. This requires high peak-power excitation lasers restricted to a small focal volume, resulting in an inherent three-dimensional (3D) sectioning capability with high spatial resolution. Coherent anti-Stokes Raman scattering[14-18] (CARS) is a multiphoton process possessing similar qualities to SHG and TPAF microscopy. However, unlike these aforementioned processes that involve electronic interactions between photon and target molecule, CARS is a vibrational imaging technique similar to its linear counterpart Raman microscopy. When the lasers are tuned to the energy of a carbon–hydrogen bond, CARS can image the signals from hydrocarbon/lipid-rich regions of living cells. This property has been used extensively to visualize biologic processes such as lipogenesis,[19] intracellular trafficking of lipids/proteins[20,21] as well as how cultured cells interact with 3D scaffolds.[22-24] CARS microscopy is not limited to cultured cells, and has been successfully used to image complex biologic tissues.[14,25-28]

In our previous work, we have shown high resolution SHG and TPAF images of the anterior chamber aqueous outflow system of human, pig, and mouse eyes.[29-31] Recently, we have imaged the human trabecular meshwork (TM) region using CARS microscopy and were able to visualize live endothelial cells.[32] That effort led to the current focus on using CARS to noninvasively image living cells of the cornea and limbus. In the present work, we successfully used CARS to image the cells and structures of an intact mouse eye and found that the images are on par with those from histologic sections, indicating that this technology can be used to generate virtual cross-sections of intact eye tissue without dependence on tissue processing.
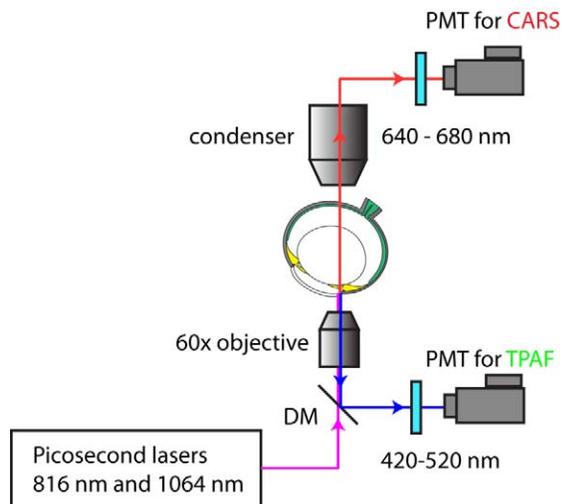
FIGURE 1. MPM setup for CARS and TPAF imaging of cornea. A picosecond laser system with an internal optical parametric oscillator generates an 816 nm and a 1064 nm laser beam to target the cornea of an intact eye. The TPAF signal (420–520 nm) is filtered by an emission filter and is detected in the epi-direction. The CARS signal (663 nm) is filtered by a narrow-band emission filter and is detected in the forward direction. DM, dichroic mirror.

MATERIALS AND METHODS

Sample Preparation

Mouse eyes were obtained as postnecropsy tissue from mice euthanized at the conclusion of other research projects. Adult albino mice with no known prevalence for corneal eye diseases (BALB/c and FVB strains) were used. All mice were between 4 and 9 months of age. Intact eyes were first enucleated under a dissecting microscope (SMZ-800 Zoom Stereo Microscope; Nikon, Inc., Melville, NY) using a pair of curved spring scissors and then excess orbital muscle tissue was subsequently removed. In the majority of experiments, BALB/c eyes were placed in glass-bottom dishes (MatTek Corporation, Ashland, MA) containing PBS (8 g/L sodium chloride, 0.2 g/L potassium phosphate monobasic, 2.16 g/L sodium phosphate dibasic heptahydrate, pH 7.4). In a single experiment, FVB eyes were exposed to hypotonic saline (a 1:1 dilution of PBS with distilled water) for 1 hour prior to imaging.

The CARS/TPAF MPM Platform

The CARS/TPAF images were acquired with a custom-built MPM platform optimized for CARS and TPAF imaging as illustrated in Figure 1.[32] The laser system (picoEMERALD; HighQ Laser, Rankweil, Austria) consisted of a diode-pumped Nd:Vanadate (Nd:YVO$_4$) picoseconds laser at a repetition rate of 80 MHz. Inside the system, some of the generated 1064 nm laser beam was redirected to a frequency doubling crystal to produce 532 nm light, which was subsequently sent into an optical parametric oscillator to convert the 532 nm laser beam into a 1 W, approximately 6 ps, 816 nm laser beam. The remaining 1064 nm beam from the Nd:Vanadate laser was then optically recombined with the 816 nm optical beam and sent into an Olympus FV-1000 confocal microscope platform (Olympus, Center Valley, PA) for CARS and TPAF imaging. The optical power at the objective was 16.5 mW for the 816 nm laser beam and 15.0 mW for the 1064 nm laser beam; both settings are below the tissue damage threshold.[28]

Imaging Mouse Tissue

Imaging was performed on an inverted microscope (Olympus FV-1000; Olympus) equipped with multiphoton imaging capability. The TPAF signal between 420 to 520 nm was filtered (hp470/100m-2p; Chroma Technology, Belows Falls, VT) and collected in epi-direction. The CARS signal generated at 663 nm was collected using an emission filter (hq660/40m-2p) located in front of the forward photo multiplier tube (PMT). The objective used in this experiment was a ×60 1.2NA water objective (UPLSAPO 60× IR W; Olympus) optimized for CARS and TPAF imaging. The pixel dwell time was 10 μs and the image pixel resolution was 800 × 800 when acquiring xy stacks and 1018 × 3000 for line scans. A Kalman average filter ($n = 3$ for xy stacks and $n = 10$ for line scans) was applied during image acquisitions to improve the signal-to-noise ratio of the acquired images.

Intact mouse eyes were placed on the microscope stage in a humidity/temperature-controlled chamber. For sagittal/transverse line-scans of the eye, enucleated mouse eyes were oriented such that the axis connecting the optic nerve and pupil pointed downward at an approximately 45° angle. This placed the microscope objective facing the corneal/limbal region of the eye (Fig. 1). For full-tissue thickness imaging of the cornea, eyes were oriented with the corneal directed approximately perpendicular to the objective lens.

Image Analysis and Processing

The Olympus FV-1000 software package (Olympus) was used to collect all images. Acquired images were postprocessed for background noise reduction and prepared in its current format by ImageJ (provided in the public domain at http://rsbweb.nih.gov/ij/; National Institutes of Health, Bethesda, MD) software. Where applicable, tiling of the line-scans was accomplished by Adobe Illustrator (Adobe, San Jose, CA).

RESULTS

Corneal Imaging

Sequential coronal images were collected through the full thickness of the cornea parallel to the surface (Figs. 2, 3). These images were used to generate a virtual cross-section of the mouse cornea. As shown in Figure 2A, the lipid within the plasma membrane of the corneal epithelium (EP) and endothelium (EN) can be detected by CARS (red signal). Multiple layers of corneal EP cells were visible within the first 30 μm of the corneal surface. This is demonstrated in Figure 2B which shows a coronal section approximately 11 μm below the surface of the cornea. The CARS signal appears as a honeycomb structure of packed rings (representing EP plasma membranes) with the dark centers. Dark spaces of approximately 5 to 7 μm are apparent and most likely represent intracellular regions lacking lipid membrane. In addition, no TPAF signal (green) from collagen or other extracellular matrix proteins was seen within the first 30 μm from the surface region of the cornea where the CARS signal was strongest, indicating this region is densely populated with corneal EP and lacks a significant amount of collagen.

In contrast, significant TPAF signal extended from approximately 30 μm to approximately 110 μm below the surface of the cornea (Fig. 2A). This approximately 80-μm thick region represents the corneal stroma (ST), which is abundant in collagen, and therefore collagen is the likely source of the TPAF signal. Figures 2C and 2D show coronal sections 38 and 90 μm below the surface, respectively. Along with the TPAF signal emitted by the collagen matrix, a few cells with strong CARS
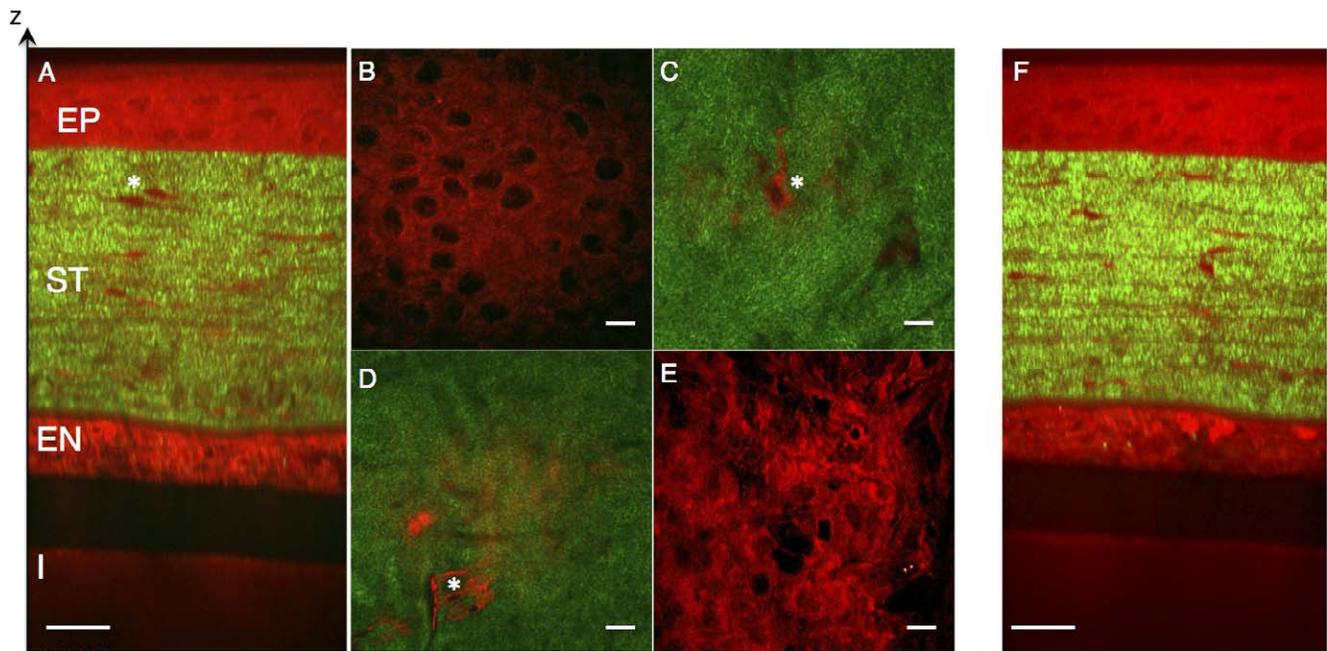
Figure 2. Multiphoton images of the mouse cornea, with CARS signal shown in *red* and TPAF shown in *green*. **(A)** has a sagittal/transverse section, showing the CARS signal from the lipid membranes of the corneal EP and corneal EN. A weaker CARS signal is detected in the I. There is a strong TPAF signal from the collagen fibers of the corneal ST. Images in **(B–E)** are coronal sections of the same region of the cornea at various depths (11, 38, 90, and 120 μm) below the surface of the EP. **(F)** is a sagittal/transverse from a second animal. CARS signal within the ST (*) may represent keratinocytes or ST fibroblasts. *Scale bars*: 20 μm.
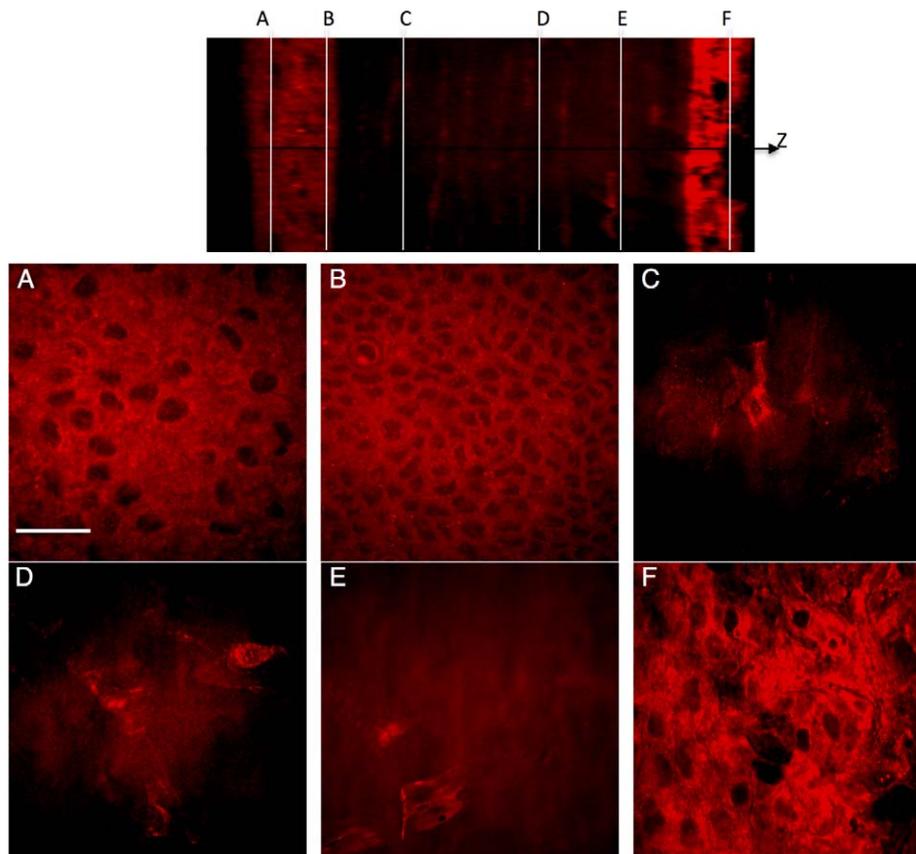
Figure 3. CARS microscopy of the mouse cornea. **(A–F)** show CARS (*red*) from individual coronal sections at various depths below the corneal surface indicated by the *white lines* in the corneal cross-section located *above*. CARS signal (*red*) from lipid membranes demonstrate the size and location of cells within the cornea. Larger cells in the corneal EP are seen closer to the surface (**[A]**, 11 μm below surface of the cornea) compared with deeper within the EP (**[B]**, 20 μm below). Keratinocytes/fibroblasts sparsely populate the corneal ST in (**C-E**) (38, 70, and 90 μm below the surface of the cornea). Cells of the EN appear as small structures between 3 and 5 μm (**[F]**, 121 μm below). *Scale bar*: 25 μm.
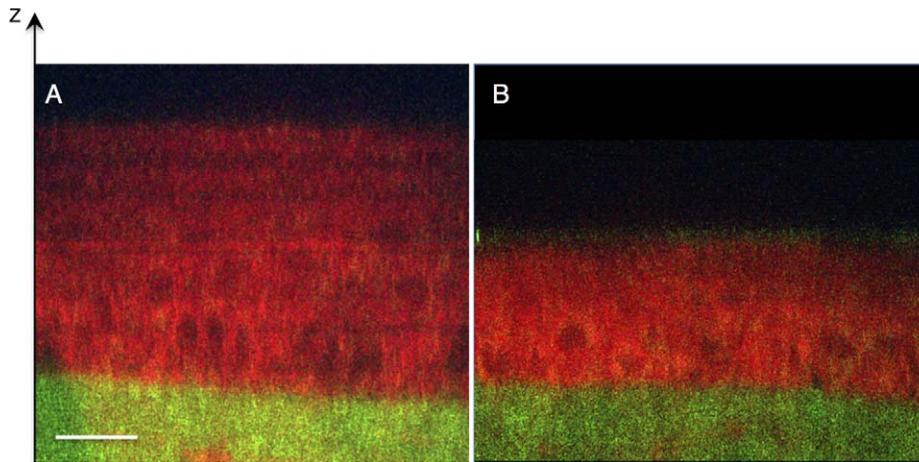
FIGURE 4. Transverse/sagittal line scans of mouse cornea exposed to hypotonic saline. Albino mouse eyes (FVB) were exposed to either hypotonic saline (**A**) or isotonic saline (**B**) for 1 hour prior to multiphoton imaging. CARS signal shown in *red* and TPAF shown in *green*. The cells of the corneal EP appear swollen after treatment with hypotonic saline (**A**).

signal were also evident (Fig. 2, asterisk). We cannot currently differentiate among the various cell types detected within the corneal ST, which include keratocytes, fibroblastic cells, bone marrow–derived cells, and mesenchymal-derived stem cells. For simplicity we will refer to these cells as keratocytes. Some of the structures revealed by the CARS signal within the ST were much larger than a cell, and may represent myelin structures of corneal nerves. The Descemet's membrane along with the corneal EN region, manifest itself with solid CARS signal through dense lipid concentration. Corneal EN cells are apparent in Figure 2E, a transverse section approximately 120 μm below the surface. Larger structures near the endothelial cell layer, which appears to be a corneal blood vessel, also emitted a significant CARS signal. One such structure is visible in a 3D rendering of the multiple corneal sections in Figure 2 and is shown in Supplementary Movie S1. The experiment shown in Figure 2A was repeated on a different day and the result is shown in Figure 2F. Taken together, these results demonstrate the specificity and reproducibility of CARS microscopy.

Corneal measurements were taken from the cross-section images shown in Figure 2, approximately midpoint between central and peripheral cornea regions. The thickness of the BALB/c cornea measured by CARS/TPAF (129.5 ± 2.1, $n = 2$) is similar to the thickness measured histologically in BALB/c (137.0 ± 14.0 μm) and C57Bl/6 (134.2 ± 12.9 μm).[33] Stromal thickness measured by CARS/TPAF (80.8 ± 7.1 μm) was also within the range previously measured in BALB/c (90.9 ± 14.8 μm) and C57Bl/6 (81.8 ± 8.1 μm). The epithelial layer measured here (28.3 μm) is between the values of central epithelial thickness (40.6 μm) and peripheral epithelial thickness (22.4 μm) measured histologically in BALB/c. This would agree with the images from Figure 2 being located between the central and peripheral cornea.

Figure 3 highlights only the CARS signal generated by the lipid membranes within the cornea. Figures 3A through 3F show individual sections at various depths within the cornea, as indicated by the white lines in the corneal cross-section located above Panels A through F. Figures 3A and 3B are coronal sections taken through the corneal EP at different depths (10 and 20 μm below the surface, respectively). The size of the EP, as indicated by the size of the circular CARS signal from the plasma membranes, is much bigger in the outer EP (>10 μm, Fig. 3A) than in the inner EP (~5 μm, Fig. 3B). CARS images taken through the cornea in Figures 3C through

3E show the presence of keratinocytes/fibroblasts. These structures varied in shape from irregular and jagged (Figs. 3C, 3E) to oval (Fig. 3D). Corneal EN cells, shown in Figure 3F, appear as small structures between 3 and 5 μm in diameter, somewhat smaller than the cells of the inner EP and less regularly shaped.

Figure 4 shows CARS/TPAF images taken from a FVB cornea, which has similar thickness as BALB/c mouse cornea,[34] after exposure to hypotonic saline. The corneal EP appears larger in hypotonic saline (Fig. 4A) than in isotonic saline (Fig. 4B), most likely due to osmotic induced swelling. The overall thickness of the EP increased from 27 μm (Fig. 4B) to 54 μm in hypotonic saline (Fig. 4A).

Single line scans were also performed along the sagittal/transverse axis of the mouse eye. Individual line scans separated by 1 μm were performed through the full thickness of the tissue, starting approximately 200 μm beyond the limbus and continuing into the cornea. This imaging was performed in three separate eyes, and a representative image is shown in Figure 5. Here the cornea was located on the left; with the CARS signal in red and TPAF in green. The thick corneal EP and the thinner corneal EP can be seen by their CARS signals, separated by the green signal from the collagen of the corneal ST. The CARS signal from the iris (I) is visible below the sclera (S) as a thin irregular line approximately 10- to 15-μm thick. As the cornea transitions to S tissue, the green TPAF signal from the collagen thins. The transition from the cornea to sclera was also marked by a change in collagen pattern (TPAF channel) and thickness of surface cells (CARS channel). While the collagen within the corneal ST appears as repeated stacks of thin sheets, the collagen fibers within the S and conjunctival substantia propria (C) are more random (Fig. 5). Many of the collagen fibers in the sclera appear bundled in long wavy structures; however, the collagen just beneath the conjunctiva cell layer is much shorter with no apparent bundling. Additionally, regions within the cornea lacking TPAF signal (collagen) almost always coincide with a strong CARS signal. In contrast, regions lacking both TPAF and CARS signal are common with the S, and likely represent fluid filled spaces that were also noted in the limbal imaging performed previously in mouse.[30]

The boxed region in Figure 5A represents the limbal region, and is shown at greater magnification in Figure 5B. Visible along the top of Figure 5B (red, CARS) is a thin layer of conjunctiva that transitions into a thicker cornea EP cells. Below these cell layers, the TPAF of the S and ST are visible in green. At the junction of the S and cornea is a region without
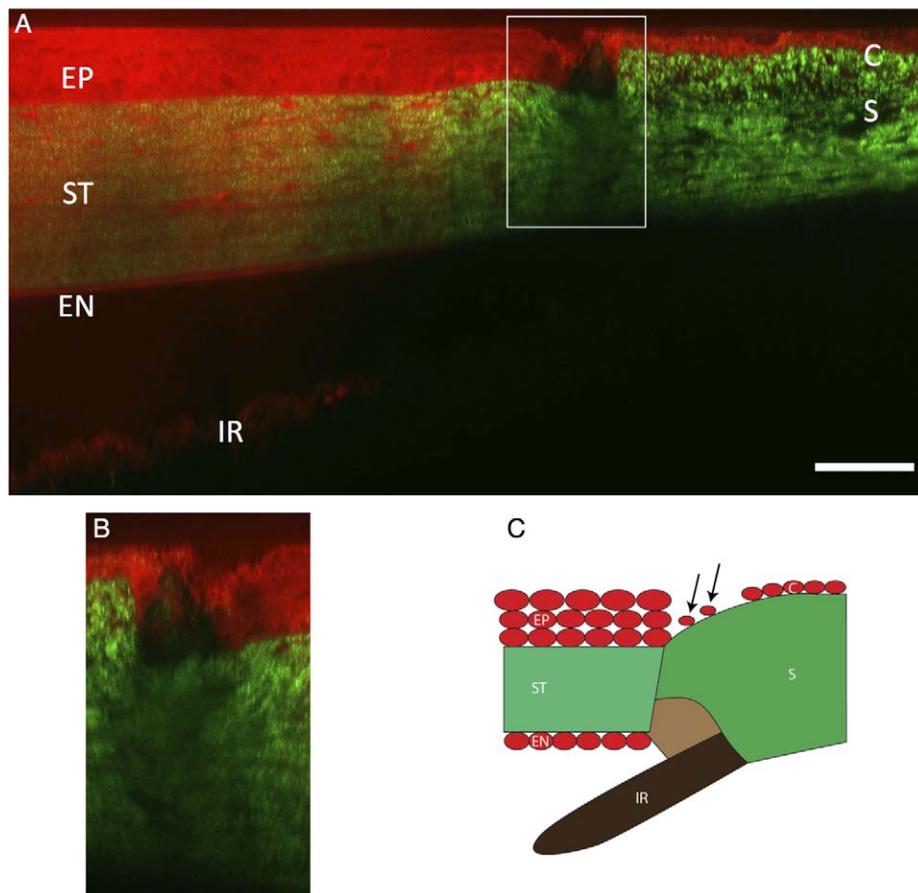
FIGURE 5. Transverse/sagittal section of the limbal region. In all panels, the cornea is oriented on the *left* with CARS signal shown in *red* and TPAF shown in *green*. (**A**) shows a line scan of the full thickness of mouse tissue centered on the limbal region of S and cornea. The collagen of the cornea (TPAF, *green*) is thicker in the cornea ST compared with the S, and the surface cell layers (CARS, *red*) of the corneal EP are thicker than the C. A higher resolution image of the limbus (*boxed*) is shown in (**B**), highlighting a "gap" between the ST and S that is sparsely populated by cells. A schematic of the tissue region is shown in (**C**), with *arrows* indicating the cells populating the "gap" of the limbus. *Scale bar*: 50 μm.

CARS/TPAF signal. This "gap" correlates to the location of the limbus, and appears to contain sporadic circular structures (red, CARS). Given the location, we speculate that these may be limbal stem cells, but we have not performed further experiments to identify these cells. Figure 5C is a diagram of the major structures of the limbal region seen with CARS/TPAF, with the limbal cells indicated by arrows.

Limbal Imaging

The limbus of mouse eyes was imaged at various depths below the surface of the tissue in order to better resolve the region shown in Figure 5B. The images shown in Figures 6A through 6F are oriented parallel to the surface of the eye, collected at various depths (4, 8, 14, 20, 26, and 32 μm, respectively) below the surface of the corneal/scleral interface. The conjunctiva/sclera is located at the top of all images, with the cornea located below. The CARS signal from the lipid membranes of the corneal EP extends approximately 26 μm below the surface of the tissue (Figs. 6A–E); in many cases the cells are shown in cross-section with a bright ring CARS signal surrounding a dark intracellular space (Figs. 6C, 6D). The CARS signal from the conjunctiva, being much thinner than the corneal EP, is evident within 4 μm of the tissue surface (Fig. 6A, top), but is absent in deeper sections. The green TPAF of the S is visible from 8 to 32 μm below the surface of the tissue (Figs. 6B–E, top), while the TPAF of the corneal ST only becomes

evident at 26 μm below the surface of the cornea (Fig. 6E, bottom). The different organization of the collagen in the S and ST is shown in Figure 6F: The collagen fibers of the S appear thicker than the fibers in the ST, while the fibers of the ST are more closely packed with fewer spaces between them. Another noticeable fact is that the green TPAF signal from the collagen fibers of the S are separated from the corneal EP by the gap of the limbus. Similar to the circular CARS structures seen in Figure 5B, occasional cells are also visible seen in this gap region (Fig. 6C, arrows). Images shown in Figure 6 are representative of images collected from three different mouse eyes. A 3D rendering of these image stacks is included in Supplementary Movie S2.

DISCUSSION

Traditional single photon microscopy, including brightfield and confocal microscopy,[35] is used in the clinical setting for imaging and diagnosis of corneal pathology such as infection and dystrophies.[13,36,37] A simple "specular" slit-lamp microscope can image the corneal endothelial cell density, and more sophisticated confocal microscopes are able imaging all layers of the cornea.[37] Both have high enough resolution to image and count individual cells. However, as with any linear microscopic technique, the contrast depends only on changes in linear refractive index. Therefore, in both of these cases any molecular specificity and functionality information is absent.
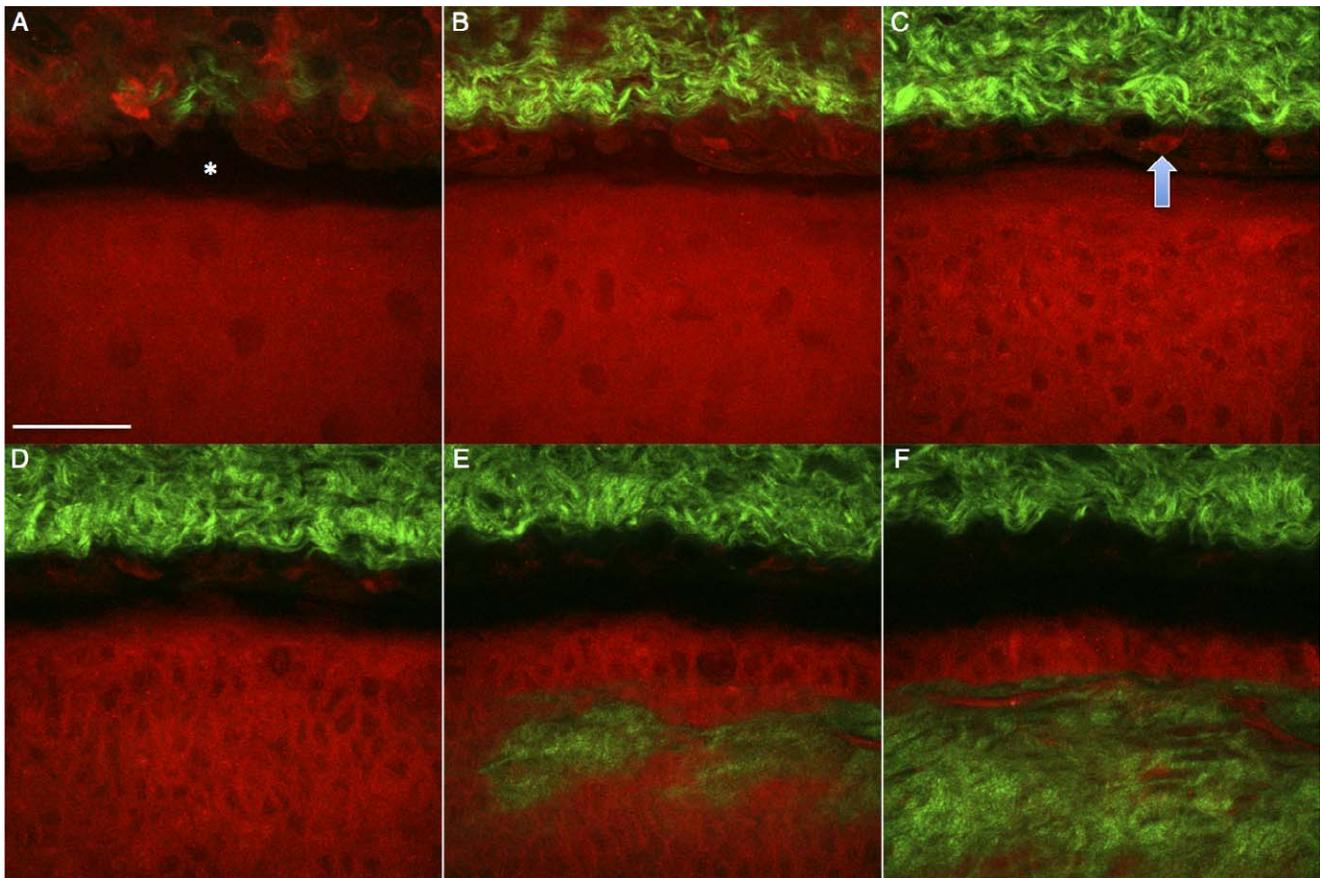
FIGURE 6. Multiphoton images of the mouse limbus. CARS signal is shown in *red* and TPAF shown in *green*. Images in (**A–F**) are sections at various depths (4, 8, 14, 20, 26, 32 μm, respectively) below the surface of the tissue. A "gap" region between the S and cornea, lacking both CARS and TPAF signal, is visible (*, [**A**]). Occasional undefined cells are seen in this "gap" region (*arrow*, [**C**]). *Scale bar*: 50 μm.

In contrast, MPM has the ability to image the function and structure of cells and tissues without exogenous dyes. This label-free imaging relies on simultaneous interactions of multiple photons with the target material. These interactions involve a resonant or nonresonant excitation of one of the basic energy states: electronic or vibrational energies. Unlike traditional microscopy where a single photon interacts with material (through scattering or absorption), MPM uses pulsed infrared laser light to generate signal from a sample through simultaneous absorption or scattering of two or more photons. In TPAF, two photons from a single laser are simultaneously absorbed and excite the molecule to its higher electronic state. After nonradiative relaxation, the molecule returns to its electronic ground state through the release of a fluorescent photon. Similar to TPAF, SHG is a two-photon process. In the case of SHG however, the interaction between the laser field and the matter is through simultaneous scattering of two photons and there is no energy transferred to the material. In CARS, two laser beams with different optical wavelengths simultaneously and resonantly excite the vibrational states of carbon–hydrogen bonds in an ensemble of lipid molecules in a coherent fashion. This ultimately results in the release of optical photons in a direction that is dependent on the size and shape of the lipid object. In most instances, however, significant CARS signal is emitted in the forward direction.[38]

In this manuscript, we demonstrate the utility of CARS to image the lipid-rich membranes of the cells covering the ocular surface as well as cells residing deeply within the tissue. To our knowledge, these findings have not been reported previously in published literature. In previous works, we and others have used TPAF to image the levels of the metabolite NAD(P)H, which can serve as a surrogate metric for the oxidative state within living cells.[3,39] We propose, therefore, that multimodal CARS/TPAF microscopy has the ability to simultaneous image the individual cell membranes (via CARS), while also determining the metabolic state (via TPAF of NAD[P]H) and tissue structure (via TPAF of collagen). CARS/TPAF has already been used to monitor drug effects in situ,[40] while the CARS-related technique (stimulated Raman scattering) has been used to detect and track the penetration of drug into the skin of live mice.[41] Additionally, CARS/TPAF leverages laser technology (816 and 1064 nm) that is already being used safely for corneal refractive surgery (1040 nm).[42,43] According to ANSI 2000,[44] which documents standards for protection of the human eye from laser exposure, wavelengths ranging from 400 to 1400 nm have the same maximum permissible exposure (Table 1 in Ref. 44). Therefore, the remaining in vivo safety concern is the energy needed for imaging. For comparison, femtosecond lasers (~500 fs) for refractive surgery typically use approximately 10^{-6} J/pulse to cut.[43,45] In our experiments, we calculate an energy of approximately 3×10^{-8} J/pulse, which is two orders of magnitude less energy used per pulse. Moreover, damages related to peak power (ionization) rather than average power are significantly reduced in picosecond pulses as the ablation threshold increases.[46]

Finally, in the images presented here, CARS signal was collected from the forward detector, which could not be

performed in a clinical application. In other experiments, however, we have imaged scleral tissue by CARS in the reflected (epi) direction.[47] Clinical CARS imaging of the cornea could be performed by capturing scattered and reflected signal from other structures inside the eye, and there are technical developments currently in progress toward this goal. We acknowledge that current translation of this technology into in vivo imaging device requires overcoming some technical hurdles including faster acquisition speed and better signal collection efficiency. However, even with this current limitation, this technique can be applied to the imaging of animal tissues today.

We believe that these imaging modalities have many potential medical applications for corneal/ocular surface imaging when the technology is further developed. Chronic topical glaucoma therapy has been associated with corneal damage characterized by the loss of certain corneal cell types as well as invasion of inflammatory cells.[48,49] CARS/TPAF would allow us to observe the number and type of corneal epithelial cells, which could determine the progression of corneal surface disease to better aid physician treatment. CARS/TPAF also has application in the area of corneal surgery, since this technology could be used to observe cell number and metabolic state (NAD[P]H level) at the site of a healing wound. Furthermore, CARS/TPAF can image at the level of the corneal endothelium to monitor cell health before and after cataract surgery. A combined CARS/TPAF system has recently been used to show the differences in lipid structures between in healthy and psoriasis-affected human skin.[50] By the same reasoning, CARS/TPAF could be the first technology to image the host/graft interaction in the case of corneal transplantation. We also believe that this technology would be well suited for use in optic biopsy. Penetrating corneal infections, while rare, are difficult to treat and can lead to loss of the eye. Diagnosis that leads to early treatment greatly improves patient outcomes; however, this is traditionally done by removal of corneal tissue, which can by itself lead to damage and scaring. CARS microscopy has been successfully used to identify small numbers ($\sim 10^4$) of bacteria with a single laser pulse.[51] If spectral signatures of specific infectious agents could be identified, then CARS/TPAF could potentially diagnose corneal infections noninvasively. In the future, CARS/TPAF imaging could be combined with surgical femtosecond lasers to provide precise localization for improved targeting and decreasing collateral damage. In conclusion, we have achieved label-free, vibrational specific, high resolution images of anterior tissue structures of the mouse eye. Along with other nonlinear modalities such as TPAF and second/third harmonic generation, CARS can add significant information about cellular structure and health that can enhance future diagnosis and management of ophthalmic diseases.

Acknowledgments

Disclosure: **D.A. Ammar**, P; **T.C. Lei**, P; **M.Y. Kahook**, P; **O. Masihzadeh**, P

References

1. Cox G, Sheppard CJ. Practical limits of resolution in confocal and non-linear microscopy. *Microsc Res Tech*. 2004;63:18–22.

2. Denk W, Strickler JH, Webb WW. Two-photon laser scanning fluorescence microscopy. *Science*. 1990;248:73–76.

3. Piston DW, Masters BR, Webb WW. Three-dimensionally resolved NAD(P)H cellular metabolic redox imaging of the in situ cornea with two-photon excitation laser scanning microscopy. *J Microsc*. 1995;178:20–27.

4. Guo YC, Ho PP, Savage H, et al. Second-harmonic tomography of tissues. *Opt Lett*. 1997;22:1323–1325.

5. Campagnola PJ, Clark HA, Mohler WA, Lewis A, Loew LM. Second-harmonic imaging microscopy of living cells. *J Biomed Opt*. 2001;6:277–286.

6. Yeh AT, Nassif N, Zoumi A, Tromberg BJ. Selective corneal imaging using combined second-harmonic generation and two-photon excited fluorescence. *Opt Lett*. 2002;27:2082–2084.

7. Zoumi A, Yeh A, Tromberg BJ. Imaging cells and extracellular matrix in vivo by using second-harmonic generation and two-photon excited fluorescence. *Proc Natl Acad Sci U S A*. 2002; 99:11014–11019.

8. Bueno JM, Gualda EJ, Artal P. Analysis of corneal stroma organization with wavefront optimized nonlinear microscopy. *Cornea*. 2011;30:692–701.

9. Morishige N, Petroll WM, Nishida T, Kenney MC, Jester JV. Noninvasive corneal stromal collagen imaging using two-photon-generated second-harmonic signals. *J Cataract Refract Surg*. 2006;32:1784–1791.

10. Lyubovitsky JG, Spencer JA, Krasieva TB, Andersen B, Tromberg BJ. Imaging corneal pathology in a transgenic mouse model using nonlinear microscopy. *J Biomed Opt*. 2006;11:014013.

11. Tan HY, Sun Y, Lo W, et al. Multiphoton fluorescence and second harmonic generation imaging of the structural alterations in keratoconus ex vivo. *Invest Ophthalmol Vis Sci*. 2006;47:5251–5259.

12. Morishige N, Yamada N, Teranishi S, Chikama T, Nishida T, Takahara A. Detection of subepithelial fibrosis associated with corneal stromal edema by second harmonic generation imaging microscopy. *Invest Ophthalmol Vis Sci*. 2009;50: 3145–3150.

13. Alhatem A, Cavalcanti B, Hamrah P. In vivo confocal microscopy in dry eye disease and related conditions. *Semin Ophthalmol*. 2012;27:143–153.

14. Evans CL, Potma EO, Puoris'haag M, Cote D, Lin CP, Xie XS. Chemical imaging of tissue in vivo with video-rate coherent anti-Stokes Raman scattering microscopy. *Proc Natl Acad Sci U S A*. 2005;102:16807–16812.

15. Zumbusch A, Holtom GR, Xie XS. Three-dimensional vibrational imaging by coherent anti-Stokes Raman scattering. *Phys Rev Lett*. 1999;82:4142–4145.

16. Volkmer A, Cheng JX, Xie XS. Vibrational imaging with high sensitivity via epidetected coherent anti-Stokes Raman scattering microscopy. *Phys Rev Lett*. 2001;87.

17. Cheng JX, Xie XS. Coherent anti-Stokes Raman scattering microscopy: instrumentation, theory, and applications. *J Phys Chem B*. 2004;108:827–840.

18. Min W, Freudiger CW, Lu S, Xie XS. Coherent nonlinear optical imaging: beyond fluorescence microscopy. *Ann Rev Phys Chem*. 2011;62:507–530.

19. Rakic B, Sagan SM, Noestheden M, et al. Peroxisome proliferator-activated receptor alpha antagonism inhibits hepatitis C virus replication. *Chem Biol*. 2006;13:23–30.

20. Nan X, Potma EO, Xie XS. Nonperturbative chemical imaging of organelle transport in living cells with coherent anti-stokes Raman scattering microscopy. *Biophys J*. 2006;91:728–735.

21. Tong L, Lu Y, Lee RJ, Cheng JX. Imaging receptor-mediated endocytosis with a polymeric nanoparticle-based coherent anti-stokes Raman scattering probe. *J Phys Chem B*. 2007;111: 9980–9985.

22. Kaufman LJ, Brangwynne CP, Kasza KE, et al. Glioma expansion in collagen I matrices: analyzing collagen concentration-dependent growth and motility patterns. *Biophys J*. 2005;89:635–650.

23. Conovaloff A, Wang HW, Cheng JX, Panitch A. Imaging growth of neurites in conditioned hydrogel by coherent anti-Stokes Raman scattering microscopy. *Organogenesis*. 2009;5:231–237.

24. Brackmann C, Esguerra M, Olausson D, et al. Coherent anti-Stokes Raman scattering microscopy of human smooth muscle cells in bioengineered tissue scaffolds. *J Biomed Opt*. 2011;16: 021115.

25. Le TT, Huff TB, Cheng JX. Coherent anti-Stokes Raman scattering imaging of lipids in cancer metastasis. *BMC Cancer*. 2009;9:42.

26. Wang HW, Le TT, Cheng JX. Label-free imaging of arterial cells and extracellular matrix using a multimodal CARS microscope. *Opt Commun*. 2008;281:1813–1822.

27. Le TT, Langohr IM, Locker MJ, Sturek M, Cheng JX. Label-free molecular imaging of atherosclerotic lesions using multimodal nonlinear optical microscopy. *J Biomed Opt*. 2007;12.

28. Potma E. Tissue imaging with coherent anti-Stokes Raman scattering microscopy. In: Srinivasan G, ed. *Vibrational Spectroscopy Imaging for Biomedical Application*. New York: McGraw-Hill Professional; 2010;319.

29. Ammar DA, Lei TC, Gibson EA, Kahook MY. Two-photon imaging of the trabecular meshwork. *Mol Vis*. 2010;16:935–944.

30. Johnson AW, Ammar DA, Kahook MY. Two-photon imaging of the mouse eye. *Invest Ophthalmol Vis Sci*. 2011;52:4098–4105.

31. Masihzadeh O, Ammar DA, Kahook MY, Gibson EA, Lei TC. Direct trabecular meshwork imaging in porcine eyes through multiphoton gonioscopy. *J Biomed Opt*. 2013;18:036009.

32. Lei TC, Ammar DA, Masihzadeh O, Gibson EA, Kahook MY. Label-free imaging of trabecular meshwork cells using coherent anti-Stokes Raman scattering (CARS) microscopy. *Mol Vis*. 2011;17:2628–2633.

33. Henriksson JT, McDermott AM, Bergmanson JP. Dimensions and morphology of the cornea in three strains of mice. *Invest Ophthalmol Vis Sci*. 2009;50:3648–3654.

34. Lively GD, Jiang B, Hedberg-Buenz A, et al. Genetic dependence of central corneal thickness among inbred strains of mice. *Invest Ophthalmol Vis Sci*. 2010;51:160–171.

35. Patel DV, McGhee CNJ. Contemporary in vivo confocal microscopy of the living human cornea using white light and laser scanning techniques: a major review. *Clin Exp Ophthalmol*. 2007;35:71–88.

36. Mayer WJ, Mackert MJ, Kranebitter N, et al. Distribution of antigen presenting cells in the human cornea: correlation of in vivo confocal microscopy and immunohistochemistry in different pathologic entities. *Curr Eye Res*. 2012;37:1012–1018.

37. Zhivov A, Stachs O, Kraak R, Stave J, Guthoff RF. In vivo confocal microscopy of the ocular surface. *Ocul Surf*. 2006;4: 81–93.

38. Potma EO, de Boeij WP, Wiersma DA. Nonlinear coherent four-wave mixing in optical microscopy. *J Opt Soc Am B*. 2000;17: 1678–1684.

39. Masihzadeh O, Ammar DA, Lei TC, Gibson EA, Kahook MY. Real-time measurements of nicotinamide adenine dinucleotide in live human trabecular meshwork cells: effects of acute oxidative stress. *Exp Eye Res*. 2011;93:316–320.

40. Le TT, Ziemba A, Urasaki Y, Brotman S, Pizzorno G. Label-free evaluation of hepatic microvesicular steatosis with multimodal coherent anti-Stokes Raman scattering microscopy. *PloS One*. 2012;7:e51092.

41. Saar BG, Contreras-Rojas LR, Xie XS, Guy RH. Imaging drug delivery to skin with stimulated Raman scattering microscopy. *Mol Pharm*. 2011;8:969–975.

42. Holzer MP, Rabsilber TM, Auffarth GU. Femtosecond laser-assisted corneal flap cuts: morphology, accuracy, and histopathology. *Invest Ophthalmol Vis Sci*. 2006;47:2828–2831.

43. Plamann K, Aptel F, Arnold CL, et al. Ultrashort pulse laser surgery of the cornea and the sclera. *J Optics-Uk*. 2010;12.

44. Delori FC, Webb RH, Sliney DH. Maximum permissible exposures for ocular safety (ANSI 2000), with emphasis on ophthalmic devices. *J Opt Soc Am A Opt Image Sci Vis*. 2007; 24:1250–1265.

45. Pepose JS, Lubatschowski H. Comparing femtosecond lasers. *Cataract & Refractive Surgery Today*. 2008;10:45–51.

46. Oraevsky AA, DaSilva LB, Rubenchik AM, et al. Plasma mediated ablation of biological tissues with nanosecond-to-femtosecond laser pulses: relative role of linear and nonlinear absorption. *Ieee J Sel Top Quant*. 1996;2:801–809.

47. Masihzadeh O, Ammar DA, Kahook MY, Lei TC. Coherent anti-Stokes Raman scattering (CARS) microscopy: a novel technique for imaging the retina. *Invest Ophthalmol Vis Sci*. 2013; 54:3094–3101.

48. Noecker RJ, Herrygers LA, Anwaruddin R. Corneal and conjunctival changes caused by commonly used glaucoma medications. *Cornea*. 2004;23:490–496.

49. Baudouin C, Labbe A, Liang H, Pauly A, Brignole-Baudouin F. Preservatives in eyedrops: the good, the bad and the ugly. *Prog Retin Eye Res*. 2010;29:312–334.

50. Breunig HG, Buckle R, Kellner-Hofer M, et al. Combined in vivo multiphoton and CARS imaging of healthy and disease-affected human skin. *Microsc Res Tech*. 2012;75:492–498.

51. Pestov D, Wang X, Ariunbold GO, et al. Single-shot detection of bacterial endospores via coherent Raman spectroscopy. *Proc Natl Acad Sci U S A*. 2008;105:422–427.